



An amperometric glucose biosensor based on a GOx-entrapped TiO₂–SWCNT composite

Nguyen Quoc Dung, Dewyani Patil, Thanh–Tung Duong, Hyuck Jung, Dojin Kim*, Soon-Gil Yoon

Department of Materials Science and Engineering, Chungnam National University, Daejeon 305-764, Republic of Korea

ARTICLE INFO

Article history:

Received 26 October 2011

Received in revised form 4 January 2012

Accepted 4 January 2012

Available online 21 January 2012

Keywords:

TiO₂/SWCNTs composite

Glucose biosensor

GOx

Amperometric response

Interference

ABSTRACT

Single-walled carbon nanotubes (SWCNT) were deposited onto indium tin oxide (ITO)-coated glass using an arc-discharge method. Titanium oxide (TiO₂) was coated onto the SWCNTs using a metal–organic chemical vapor deposition (MOCVD) technique. The surface morphology and crystal structure of a TiO₂–SWCNT nanowire structured composite was investigated using FESEM, XRD and Raman spectra. The TiO₂–SWCNT composite film was used to immobilize glucose oxidase (GOx). The immobilization of GOx onto TiO₂–SWCNT composite film was characterized by FTIR spectroscopy. The glucose-sensing properties of a GOx/TiO₂–SWCNT/ITO electrode was studied at –0.25 V, and it showed a linear range of detection from 10 μM to 1.40 mM in a response time of 9 s with a low detection limit of 10 μM and a sensitivity of 5.32 μA mM^{–1} cm^{–2}. The Michaelis–Menten constant was 0.83 mM. The effects of interfering species like uric acid, ascorbic acid and sucrose were also studied.

© 2012 Elsevier B.V. All rights reserved.

1. Introduction

Glucose biosensors have attracted much attention in recent years, due to applications in a variety of fields such as medicine, food quality control and environmental monitoring [1–6]. Recently, porous nanostructured materials have attracted attention in the field of enzyme-immobilized biosensors, as they provide a suitable matrix for enzyme immobilization, and because they prevent the leaching of enzymes. Some porous materials, such as mesoporous titanium dioxide (TiO₂) films on fluorine-doped tin oxide coated glass [7], mesoporous organosilicas [8], and nanoporous cerium oxide thin film on platinum [9], are used for the immobilization of enzymes. TiO₂ is a metal oxide-type semiconductor material. The rutile and anatase phases of TiO₂ have band gaps of 3.0 and 3.2 eV, respectively, which allows various applications in the field of photocatalysis [10]: dye-sensitized solar cells [11], gas sensors [12] and electrochromic devices. In recent years, because of its biocompatibility, nontoxicity and promising enzyme catalytic properties, TiO₂ has been used as an additive in toothpaste and beauty products [13] as well as in the field of enzymatic glucose biosensors [14,15].

Carbon nanotubes (CNTs) provide a porous structure and remarkable physical, mechanical and unique electrochemical properties [16]. CNTs are, therefore, an attractive material for use in Li ion batteries [17], supercapacitors [18], gas sensors [19], humidity sensors [20], biosensors [21], and solar cells [22].

TiO₂/CNT composites show promise for use as biosensors due to interesting properties such as a high surface area and electrocatalytic properties that make them a suitable matrix for the immobilization of biomolecules. TiO₂/CNT composites have been used as cancer cell detection biosensors [23], and few reports have detailed their use as composites for glucose biosensors. Tasviri et al. reported the synthesis of MWCNT-coated TiO₂ nanoparticles using a chemical method followed by functionalization treatment using 3-aminopropyl (triethoxysilane) (APTES) at room temperature for 48 h and drying at 100 °C. To prepare GOx/NH₂–TiO₂–MWCNT, a glucose sensor electrode, NH₂–TiO₂–MWCNT, was mixed with GOx in PBS (pH 7.4) and dropped onto a glassy carbon electrode. The glucose sensing properties of GOx/NH₂–TiO₂–MWCNT/GCE were studied at –0.35 V, and showed a linear range of detection from 1.8 μM to 266 μM, with a sensitivity of 7 μA mM^{–1} and a Michaelis–Menten constant of 8.59 mM [24].

The present study reports the synthesis of a TiO₂–SWCNT composite on ITO for immobilization of GOx using a simple physical adsorption method for glucose sensing applications. The SWCNTs were deposited onto ITO using a simple arc discharge method at room temperature, followed by the deposition of TiO₂ via MOCVD to form TiO₂–SWCNT/ITO. We explored the electrochemical properties of a TiO₂/SWCNT/ITO electrode in the presence of H₂O₂ and interfering species like ascorbic acid (AA), uric acid (UA), and sucrose. The effects of working potential on responses of TiO₂–SWCNT/ITO and GOx/TiO₂–SWCNT/ITO electrodes were investigated in the presence of H₂O₂ and glucose, respectively. The results of the glucose-sensing mechanism and performance of the GOx/TiO₂–SWCNT/ITO biosensor based on working potential,

* Corresponding author. Tel.: +82 42 821 6639; fax: +82 42 823 7648.
E-mail address: dojin@cnu.ac.kr (D. Kim).

linear range of detection, limit of detection, Michaelis–Menten constant, and the response time are presented and discussed.

2. Experimental

2.1. Materials

Analytical reagent (AR) grade chemicals were used throughout the present study. De-ionized water was used throughout the experiments. Glucose oxidase (GOx) (EC1.1.3.4, from *Aspergillus niger*, 200 units/mg), AA and D-glucose were purchased from Sigma. Ti(IV) di-isopropoxidediisobutylmethanato [Ti(O-iPr)₂(dibm)₂] precursor was purchased from Kojundo Chemical Lab Co. Ltd., Japan, and was used as the TiO₂ source. UA was obtained from Alfa Aesar. The other chemicals, potassium dihydrogen orthophosphate (KH₂PO₄), dipotassium hydrogen orthophosphate (K₂HPO₄), and sucrose, were obtained from DAE JUNG Reagents Chemicals, Korea. All electrochemical experiments were carried out in a 0.1 M phosphate buffer saline (PBS) prepared from K₂HPO₄ (0.075 M) and KH₂PO₄ (0.025 M), and the pH was adjusted to 7.0. ITO-coated glass substrates (size ~0.5 cm × 2.0 cm) were cut from an ITO-coated glass sheet (size – 30 cm × 40 cm and 1.1 mm thick) with a sheet resistance of ~6.5 Ω/□, that was procured from Samsung Corning Co. Ltd., Korea.

2.2. Preparation of TiO₂–SWCNT/ITO electrodes

SWCNTs were grown onto ITO substrates using an arc-discharge method at an arcing current density of 40 A cm⁻² in ambient H₂ at 400 Torr for 4 min. A graphite rod containing catalyst metal wires of Ni, Fe and Mo was used as a carbon source. The substrate temperature was kept at room temperature. ITO substrates were ultrasonically cleaned in methanol, acetone and de-ionized water for 10 min each and dried in nitrogen gas flow prior to use. The deposited SWCNTs were used as a template for the deposition of TiO₂ via MOCVD. For deposition of the TiO₂ layer, the titanium source, Ti(O-iPr)₂(dibm)₂ (0.075 mol L⁻¹), precursor was dissolved in hexane (0.05 mol L⁻¹) and passed through carrier argon gas (flow rate 100 sccm). The O₂ reaction gas was supplied at a fixed-flow rate of 100 sccm. The source vapor temperature was maintained at 240–300 °C, and the substrate temperature was kept at 400 °C. To prepare the GOx/TiO₂/ITO electrode, TiO₂ film without SWCNTs was deposited onto ITO without SWCNTs under the same conditions.

2.3. Immobilization of enzyme GOx

To immobilize GOx in the TiO₂–SWCNT/ITO film, 0.25 cm² was selected as the working area by covering the excess area by insulating epoxy. The GOx solution was prepared by dissolving 10 mg GOx in 1 mL phosphate buffer solution (0.1 M, pH 7.0). The TiO₂–SWCNT/ITO film was immersed in the GOx solution overnight at room temperature. The GOx/TiO₂–SWCNT/ITO electrode was then rinsed with PBS (0.1 M, pH 7.0) to remove the free enzyme, and dried at room temperature for 2 h to evaporate the solvent. The GOx-immobilized TiO₂–SWCNT/ITO electrode was stored at 4 °C in the dark when not in use.

2.4. Preparation of the glucose solution

A glucose stock solution (5 mM, 50 mM, 0.250 M and 0.5 M) was prepared in 0.1 M phosphate buffer saline (pH 7.0) and left at room temperature for about 24 h prior to use. This ensured the presence of β-D-glucose.

2.5. Electrochemical measurements

The electrochemical measurements were carried out in a 3-electrode setup with GOx/TiO₂–SWCNT/ITO as the working electrode, platinum mesh as the counter electrode, and a saturated calomel electrode (SCE) as the reference electrode. PBS (0.1 M, pH 7.0) was used as an electrolyte during the electrochemical studies. Amperometric and cyclic voltammetric measurements were carried out using a potentiostat/galvanostat (EG and G Princeton Research Model 263A, USA) controlled by electrochemistry software Powersuite 2.55.

2.6. Characterization techniques

The TiO₂–SWCNT/ITO film was characterized by X-ray diffraction (XRD). The XRD analysis was performed with a Bruker diffractometer (D8, Advance, Bruker AXS model) with CuK_α radiation (λ = 1.5406 nm) operating at 40 kV and 40 mA. The SWCNTs/ITO and TiO₂–SWCNT/ITO films were characterized by Raman spectroscopy. The Raman spectra were obtained using a Hoiba Jobin Yvon model LabRam (HR) at room temperature with 541.5 nm incident photons from an Ar ion laser in a back-scattering geometry. The surface morphology of the TiO₂–SWCNT/ITO film was investigated by field-emission scanning electron microscopy (FESEM). The FESEM analysis was carried out with a JEOL (JSM-7000F, JEOL, Japan) microscope. The TiO₂–SWCNT/ITO and GOx-immobilized TiO₂–SWCNT/ITO films were characterized by Fourier transform infrared spectroscopy (FTIR). The FTIR spectroscopy analysis was performed with a Bio-Rad spectrometer (FTS-7, Bio-Rad Laboratories Inc., USA) in the 4000–500 cm⁻¹ spectral range.

3. Results and discussion

3.1. Characterization of SWCNTs and TiO₂–SWCNT/ITO films

The XRD pattern of the TiO₂–SWCNT/ITO film [Fig. 1] shows the diffraction peaks at 2θ values of 25.28° and 37.80°, which corresponded to the anatase phase of TiO₂ with a tetragonal structure (JCPDS # 21-1272). The other diffraction peaks appeared at 2θ values of 21.64°, 30.66°, 35.56°, 45.64°, and 50.96° were related to the substrate ITO [25].

The Raman spectra of SWCNTs [Fig. 2(a)] exhibited a broad peak at 189 cm⁻¹, which was associated with the radial breathing mode (RBM). Its peak position was related to the SWCNT diameter [26]. The tube diameter was calculated using the following formula.

$$\bar{\nu}(\text{cm}^{-1}) = \frac{223.75}{d} \text{ nm} \quad (1)$$

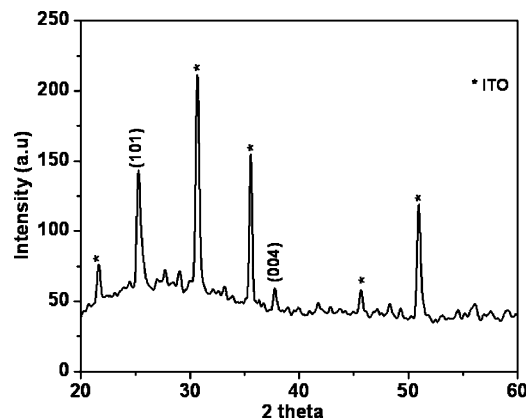


Fig. 1. X-ray diffraction pattern of a TiO₂–SWCNT/ITO electrode.

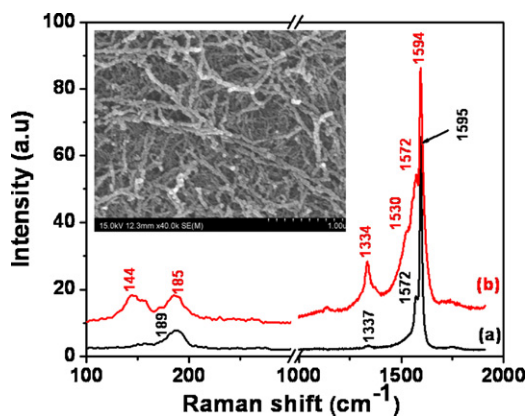


Fig. 2. Raman spectra of (a) SWCNTs and (b) TiO₂-SWCNT. The inset shows an FESEM image of the TiO₂-SWCNT/ITO electrode.

where, $\bar{\nu}$ is the wavenumber of the peak position and d is the diameter of SWCNT. The calculated diameter of SWCNT was ~ 1.18 nm. The weak peak appeared at 1337 cm^{-1} (D band), and can be attributed to the defect-induced carbon in SWCNTs. The G band of SWCNTs was split into 2 peaks: a strong peak (G^+) at 1595 cm^{-1} with a shoulder peak (G^-) at 1572 cm^{-1} . The G^+ and G^- bands are originated from longitudinal (LO) and tangential (TO) modes of SWCNT and their relative intensity depended on the chirality of the SWCNTs [27]. The intense G band with respect to the D band showed the highly crystalline graphitic nature of SWCNTs.

The Raman spectra of TiO₂-deposited SWCNTs [Fig. 2(b)] showed characteristic bands at 185, 1334, 1572 and 1594 cm^{-1} , which were similar to those of the SWCNTs. The spectrum also indicated the presence of a band at 144 cm^{-1} which corresponded with the anatase phase of TiO₂ [28]. A more intense D band was observed in TiO₂-deposited SWCNTs than in pure SWCNTs, which may have corresponded with the functionalization of SWCNTs and the coating of TiO₂ particles at a higher substrate temperature. The shoulder peak at 1530 cm^{-1} may have corresponded with a structural disorder in nanotubes due to the deposition of TiO₂. The inset in Fig. 2 shows the FESEM image of the TiO₂-SWCNT/ITO film with a highly porous nanowire structure. These results reveal that the deposition of anatase-phase TiO₂ on SWCNTs forms a porous nanowire composite.

3.2. Characterization of TiO₂-SWCNT/ITO and GOx/TiO₂-SWCNT/ITO electrodes

The FTIR spectra of TiO₂-SWCNT/ITO and GOx-immobilized TiO₂-SWCNT/ITO films are shown in Fig. 3. The FTIR spectrum of TiO₂-SWCNT/ITO film [Fig. 3(a)] exhibited a band around 3227 cm^{-1} attributed to the stretching vibrational mode of the O–H group bonded to TiO₂. The weak band at 1653 cm^{-1} and 1541 cm^{-1} corresponded to the bending vibration band of the surface attachment of an –OH group to TiO₂ and to the carbon skeleton stretching vibrations of SWCNTs [29]. The broad band at $\sim 722\text{ cm}^{-1}$ was assigned to the characteristic vibrational modes of TiO₂. The bands that appeared at 2359 and 2360 cm^{-1} in the TiO₂-SWCNT/ITO and GOx-immobilized TiO₂-SWCNT/ITO spectra, respectively, corresponded to the presence of CO₂ due to contamination from the atmosphere.

The FTIR spectrum of GOx-immobilized TiO₂-SWCNT/ITO [Fig. 3(b)] showed a shift in the characteristic bands to lower wave numbers, due to the incorporation of GOx. The bands at ~ 2923 and 667 cm^{-1} , corresponded to the stretching vibrational mode of the O–H group bonded to TiO₂ and to the characteristic vibrational mode of TiO₂, respectively. The bands present at around 1652

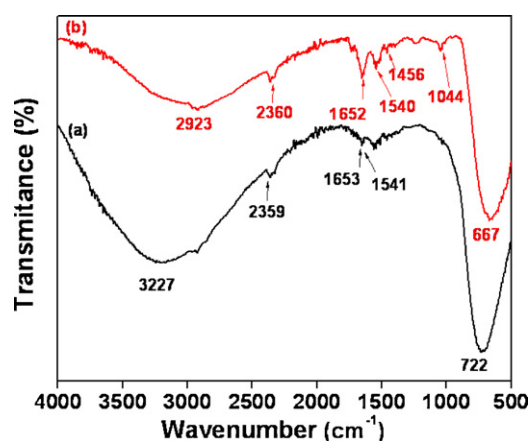


Fig. 3. FTIR spectra of (a) TiO₂-SWCNT/ITO and (b) GOx/TiO₂-SWCNT/ITO electrodes.

and 1540 cm^{-1} became more intense, and this corresponded to the C–O stretching vibration of amide I and the C–N stretching and N–H plane bending of the amide II groups present in the GOx enzyme, respectively. Thus, the FTIR spectroscopy results indicated an immobilization of GOx in the TiO₂-SWCNT/ITO film.

3.3. Electrochemical studies

The cyclic voltammetric measurements of TiO₂-SWCNT/ITO, SWCNT/ITO and GOx/TiO₂-SWCNT/ITO electrodes were recorded in 0.1 M PBS (pH 7.0) by continuously cycling the electrode potential between -0.5 V and 0.8 V versus SCE at a potential scan rate of 0.05 V s^{-1} , and are shown in Fig. 4. Fig. 4A shows the cyclic voltammogram of a TiO₂-SWCNT/ITO electrode recorded in PBS (curve a), AA 0.2 mM (curve b), UA 0.2 mM (curve c), H₂O₂ 1 mM (curve d), and oxygen (curve e). The inset of Fig. 4A shows a cyclic voltammogram of SWCNT/ITO in PBS (curve f) and in 1 mM H₂O₂ (curve g). The cyclic voltammogram of the TiO₂-SWCNT/ITO electrode in the presence of interfering species AA (curve b), and UA (curve c), showed oxidation peaks at 0.2 V and 0.3 V, respectively [30]. The oxidation current density started to increase from 0 V to 0.2 V in the presence of AA and UA, respectively. The presence of AA and UA shows no change in current density between the potential from 0 to -0.5 V by comparison with the cyclic voltammogram recorded in PBS (curve a).

The cyclic voltammogram of the TiO₂-SWCNT/ITO electrode recorded in the presence of H₂O₂ (curve d), showed considerable electrocatalytic behavior. The TiO₂-SWCNTs/ITO electrode showed increased current density after the addition of 1 mM H₂O₂ by comparison with the SWCNT/ITO electrode, which revealed that the TiO₂-SWCNT/ITO composite electrodes enhanced the H₂O₂ catalytic properties to a greater degree compared with the SWCNT/ITO electrodes. The electrocatalytic behavior of TiO₂-SWCNTs toward H₂O₂ at a positive potential can be explained by reaction (2) and at a negative potential by reaction (3):



The effect of oxygen on the TiO₂-SWCNT/ITO electrode was also investigated [curve (e)]. The reduction of oxygen species by TiO₂-SWCNTs resulted in a decrease in current density at a potential of less than -0.3 V . The TiO₂-SWCNTs/ITO electrode showed poorer catalytic activity to oxygen than to H₂O₂. The obvious electrocatalytic behavior of TiO₂-SWCNT/ITO film toward H₂O₂ showed that TiO₂-SWCNT can detect enzymatically generated H₂O₂. Therefore, the glucose biosensor was developed

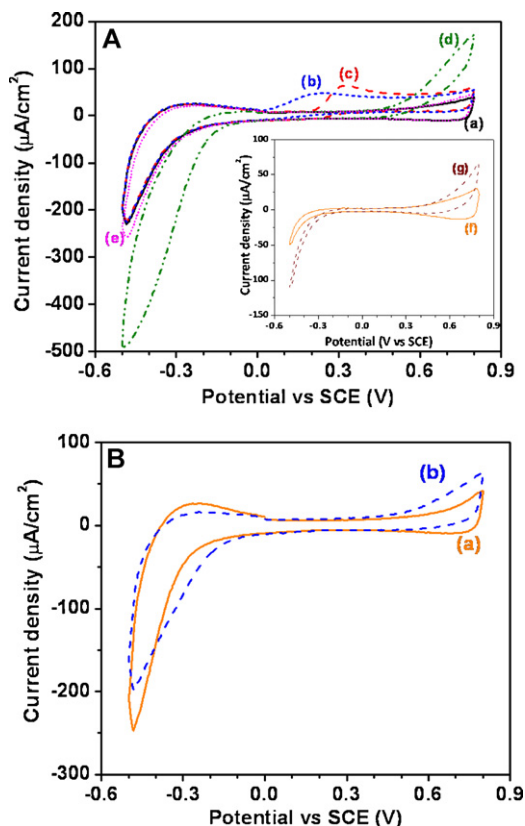


Fig. 4. (A) Cyclic voltammograms of the TiO₂-SWCNT/ITO electrode recorded in (a) PBS and in the presence of (b) AA (0.2 mM), (c) UA (0.2 mM), (d) H₂O₂ (1 mM) and (e) oxygen. Inset shows cyclic voltammograms of the SWCNT/ITO electrode recorded in (f) PBS and (g) in the presence of H₂O₂ (1 mM) in PBS. (B) Cyclic voltammograms of the GOx/TiO₂-SWCNT/ITO electrode recorded in (a) PBS and (b) in the presence of 2 mM glucose.

by the immobilization of GOx into a TiO₂-SWCNT/ITO film. To confirm the adsorption of GOx, the cyclic voltammograms of a GOx/TiO₂-SWCNT/ITO electrode were recorded in PBS (curve a) and in the presence of 2 mM of glucose (curve b), as shown in Fig. 4B. In a comparison, the cyclic voltammogram recorded in glucose showed a decrease in current density between the potentials of -0.15 V and -0.45 V during negative applied potential, and the current density increased from 0.45 V during positive applied potential. The glucose sensing mechanism of the GOx/TiO₂-SWCNT/ITO electrode can be explained by the electron

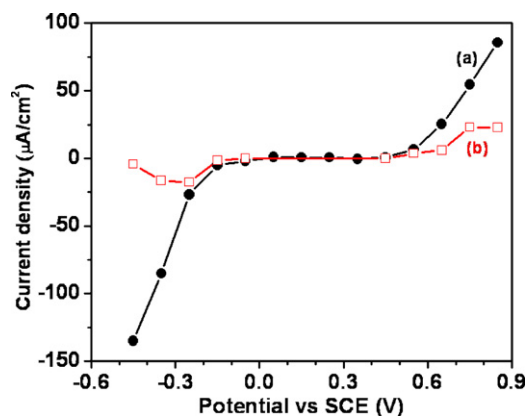
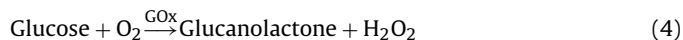


Fig. 5. Hydrodynamic voltammogram of (a) a TiO₂-SWCNT/ITO electrode to 1 mM H₂O₂ and (b) a GOx/TiO₂-SWCNT/ITO electrode to 1 mM glucose in PBS.

transfer between enzymatically generated H₂O₂ (reaction (4)) and a TiO₂-SWCNT composite.



3.4. The effect of potential on glucose sensing for a GOx/TiO₂-SWCNT/ITO electrode

The hydrodynamic voltammogram of TiO₂-SWCNT/ITO (a) and GOx/TiO₂-SWCNT/ITO electrodes (b) in the presence of 1 mM H₂O₂ and glucose, respectively, was obtained by applying different potentials from -0.45 to 0.85 V in increments of 0.1 V versus SCE, shown in Fig. 5. For amperometric measurement at each potential, fresh PBS and electrodes were employed. The TiO₂-SWCNT/ITO and GOx/TiO₂-SWCNT/ITO electrode showed a response to H₂O₂ and glucose at an applied potential of less than -0.15 V during a negative applied potential and at more than 0.55 V during a positive applied potential. The GOx/TiO₂-SWCNT/ITO electrode showed maximum change in response to a current density of 1 mM glucose at -0.25 and 0.75 V. During negative applied potential the response current density became negligible at -0.45 V, which may have corresponded to a decreased sensitivity toward glucose, which was probably due to the interference of oxygen and/or the reduction in oxygen and in PBS [Fig. 4A(e) and a)]. During a positive applied potential, the response current density plateaued at a potential that was higher than 0.75 V. Therefore, to investigate further biosensing properties, the potentials of -0.25 and 0.75 V can be applied to a GOx/TiO₂-SWCNT/ITO electrode.

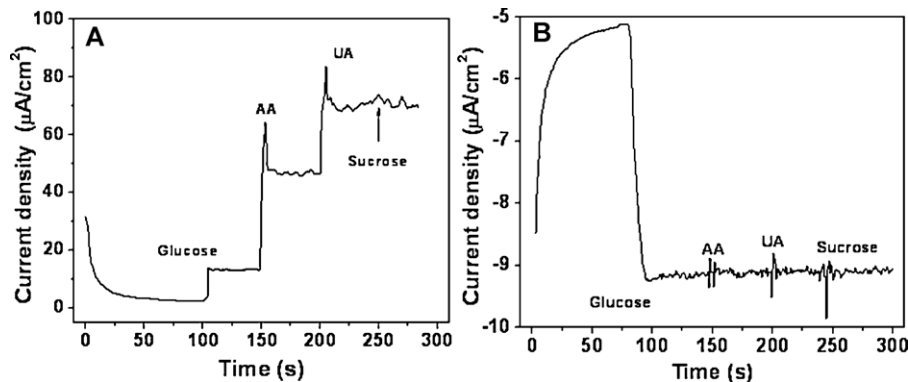


Fig. 6. Specificity of the GOx/TiO₂-SWCNT/ITO electrode to AA (0.2 mM), UA (0.2 mM), and Sucrose (0.5 mM) in the presence of 1 mM glucose in PBS at (A) 0.75 V and (B) -0.25 V.

3.5. Specificity of the GOx/TiO₂-SWCNT/ITO electrode

The effect of potential revealed 2 optimal potentials that could be used to investigate the biosensing properties of a GOx/TiO₂-SWCNT/ITO electrode, but a cyclic voltammetric study of a TiO₂-SWCNT/ITO electrode [Fig. 4(b and c)] showed the oxidation of interfering species AA and UA at positive potentials of 0.2 and 0.3 V and a reduction in oxygen below -0.3 V. Therefore, to observe the effect of AA, UA and sucrose, the specificity of the GOx/TiO₂-SWCNT/ITO electrode was evaluated at -0.25 and 0.75 V, as shown in Fig. 6. For amperometric measurement, the interfering species AA (0.2 mM), UA (0.2 mM) and sucrose (0.5 mM) were added in the presence of 1 mM glucose at intervals between 50 and 100 s. At an applied potential of 0.75 V [Fig. 6A], the GOx/TiO₂-SWCNT/ITO electrode showed a large change in current density after the addition of AA and UA, and almost no change in current density due to sucrose in the presence of 1 mM glucose. The amperometric response of the GOx/TiO₂-SWCNT/ITO electrode at -0.25 V [Fig. 6B] showed no change in current density after the addition of AA, UA and sucrose in the presence of 1 mM glucose, which showed a high selectivity for a glucose substrate. Therefore, a potential of -0.25 V can be used as a suitable potential for the detection of glucose with high specificity for the GOx/TiO₂-SWCNT/ITO electrode.

3.6. Amperometric response of the GOx/TiO₂-SWCNT/ITO electrode

The steady-state amperometric responses of the GOx/TiO₂/ITO, GOx/SWCNT/ITO, and GOx/TiO₂-SWCNT/ITO electrodes, recorded at a potential of -0.25 V (versus SCE) in PBS after successive additions of different concentrations of glucose aliquots are shown in Fig. 7. Fig. 7A shows the response current density of a GOx/SWCNT/ITO electrode to be higher than that of the GOx/TiO₂/ITO electrode. Fig. 7B, however, shows that the response of the GOx/TiO₂-SWCNT/ITO electrode was much higher than that of either of the electrodes in Fig. 7A. This visible enhancement can be attributed to the large surface area of the GOx/TiO₂-SWCNT/ITO electrode. The response of the GOx/TiO₂-SWCNT/ITO electrode to 1 mM of glucose was 685 times higher than that of the GOx/TiO₂/ITO electrode. As shown in the inset of Fig. 7B, the minimum glucose concentration that the GOx/TiO₂-SWCNT/ITO electrode could detect was $10 \mu\text{M}$. The electrode also achieved a 90% steady-state current within 9 s, which indicated a fast electron transfer between enzymatically generated H₂O₂ and TiO₂/SWCNTs.

The steady-state amperometric responses were used to construct a calibration curve of the GOx/TiO₂-SWCNT/ITO electrode, which is presented in Fig. 8(a). The error bar indicates the standard error in the responses measured for 3 different electrodes, and shows that the GOx/TiO₂-SWCNT/ITO electrode exhibited good linearity for glucose sensing from $10 \mu\text{M}$ to 1.42 mM with a correlation coefficient of 0.99. The sensitivity of the GOx/TiO₂-SWCNT/ITO electrode calculated from the slope of the calibration curve was $5.32 \mu\text{A mM}^{-1} \text{cm}^{-2}$. The experimentally measured limit of detection for glucose was $10 \mu\text{M}$ for the GOx/TiO₂-SWCNT/ITO electrode.

The apparent Michaelis–Menten constant (K_m) and maximum response current density were calculated for the immobilized GOx using an Eadie–Hofstee plot [31], and the ratio of the response current density to glucose concentration was obtained using the data presented in Fig. 8(a) for the GOx/TiO₂-SWCNT/ITO electrode that is shown in Fig. 8(b). The K_m values and the maximum response current density were calculated from the linear region of this plot. The values of the maximum response current density and K_m calculated from the Eadie–Hofstee plot for the GOx/TiO₂-SWCNT/ITO electrode were $20.03 \mu\text{A cm}^{-2}$ and $K_m = 0.83$ mM, respectively, which were nearly similar to the values calculated using a

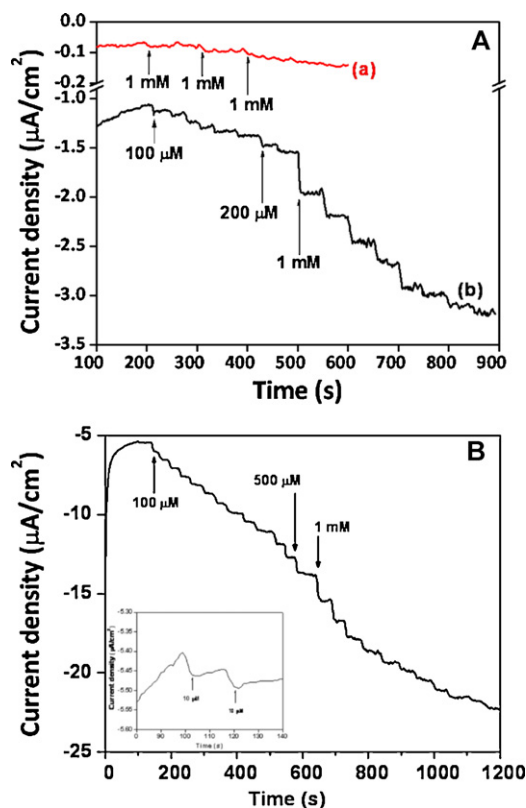


Fig. 7. Amperometric responses of (A) GOx/TiO₂/ITO (a) and SWCNT/ITO (b) electrodes, and (B) GOx/TiO₂-SWCNT/ITO electrodes measured at -0.25 V (versus SCE) with successive additions of glucose aliquots in PBS. Inset of (B) shows the amperometric response of the GOx/TiO₂-SWCNT/ITO electrode after the addition of $10 \mu\text{M}$ glucose aliquots in PBS.

Lineweaver–Burk plot at $19.23 \mu\text{A cm}^{-2}$ and 0.71 mM, respectively. The low K_m value can be attributed to the great affinity between the enzyme and the electrode. Comparisons of our results based on the applied potential, K_m , linear range of detection, and limits of detection with other glucose biosensors are shown in Table 1. These results show that the GOx/TiO₂-SWCNT/ITO electrode exhibited relatively improved characteristics in terms of applied potential, K_m and limits of detection.

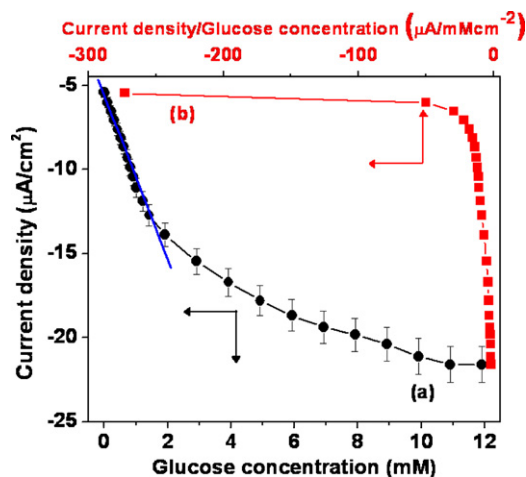


Fig. 8. (a) Calibration curve of the GOx/TiO₂-SWCNT/ITO electrode and (b) the Eadie–Hofstee plot for the GOx/TiO₂-SWCNT/ITO electrode.

Table 1
Performance comparison of the GOx/TiO₂-SWCNT/ITO electrode with published glucose sensing electrodes.

Immobilization matrix	Applied potential (V)	K _m (mM)	Linear range (mM)	Limit of detection (μM)	Reference
TiO ₂	-0.45	-	0.15–1.2	0.15	[13]
Pt-CNT/TiO ₂	0.4	-	0.010–1.5	5.7	[34]
AuNPs-TiO ₂ NT	0.25	7.2	0.40–8	310	[33]
NH ₂ -TiO ₂ -CNTs	-0.35	8.59	0.0018–0.266	0.44	[24]
TiO ₂ on FTO	0.55	3.76	0.153–1.30	51	[14]
ZnO nanorods	0.8	1.95	0.01–0.25 and 0.3–0.7	10	[32]
Pt-CNTs	-0.1	2.6	0.16–11.5	55	[35]
Nafion-GOx-SWCNTs	0.3	8.5	0–6	6	[36]
TiO ₂ -SWCNT NWS	-0.25	0.71	0.010–1.42	10	Our work

4. Conclusions

A highly porous TiO₂-SWCNT/ITO electrode was successfully fabricated by the deposition of SWCNTs on ITO using a simple arc discharge followed by TiO₂ coating via MOCVD. The highly selective and sensitive electrocatalytic activity of TiO₂-SWCNT/ITO electrodes facilitates the sensitive detection of enzymatically generated H₂O₂. The electrocatalytic behavior of the TiO₂-SWCNT/ITO and GOx/TiO₂-SWCNT/ITO electrode toward H₂O₂ and glucose shows that -0.25 V is a suitable potential to investigate interference-free biosensing properties. The GOx/TiO₂-SWCNT/ITO electrode demonstrated relatively better glucose-sensing properties such as a linear range of detection from 10 μM to 1.42 mM with lower limits of detection at 10 μM and a sensitivity of 5.32 μA mM⁻¹ cm⁻². This electrode showed a lower Michaelis-Menten constant of 0.83 mM. The present study showed that the nanowire-structured TiO₂-SWCNT composite is a high porosity material that shows great promise for use as a glucose biosensor.

Acknowledgments

This research was supported by the National Research Laboratory and WCU (R32-20026) programs of the Ministry of Education, Science and Technology of Korea.

References

- [1] Z.W. Zhao, X.J. Chen, K. Tay, J.S. Chen, Z.J. Han, K.A. Khor, A novel amperometric biosensor based on ZnO:Co nanoclusters for biosensing glucose, *Biosens. Bioelectron.* 23 (2007) 135–139.
- [2] Y.T. Wang, L. Yu, Z.Q. Zhu, J. Zhang, J.Z. Zhu, C.H. Fan, Improved enzyme immobilization for enhanced bioelectrocatalytic activity of glucose sensor, *Sens. Actuators B: Chem.* 136 (2009) 332–337.
- [3] Y. Lei, X. Yan, N. Luo, Y. Song, Y. Zhang, ZnO nanotetrapod network as the adsorption layer for the improvement of glucose detection via multiterminal electron-exchange, *Colloids Surf. A* 361 (2010) 169–173.
- [4] Y. Wei, Y. Li, X. Liu, Y. Xian, G. Shi, L. Jin, ZnO nanorods/Au hybrid nanocomposites for glucose biosensor, *Biosens. Bioelectron.* 26 (2010) 275–278.
- [5] X. Jiang, Y. Wu, X. Mao, X. Cui, L. Zhu, Amperometric glucose biosensor based on integration of glucose oxidase with platinum nanoparticles/ordered mesoporous carbon nanocomposite, *Sens. Actuators B: Chem.* 153 (2011) 158–163.
- [6] T. Hoshino, S.I. Sekiguchi, H. Muguruma, Amperometric biosensor based on multilayer containing carbon nanotube, plasma-polymerized film, electron transfer mediator phenothiazine, and glucose dehydrogenase, *Bioelectrochemistry* 84 (2012) 1–5.
- [7] S. Cosnier, C. Gondran, A. Senillou, M. Gratzel, N. Vlachopoulos, Mesoporous TiO₂ thin films: new catalytic electrode materials for fabricating amperometric biosensors based on oxidases, *Electroanalysis* 9 (1997) 1387–1391.
- [8] Z. Zhou, N. Robin, K. Taylor, S. Kullmann, H. Bao, M. Hartmann, Mesoporous organosilicas with large cage-like pores for high efficiency immobilization of enzymes, *Adv. Mater.* 23 (2011) 2627–2632.
- [9] S. Saha, S.K. Arya, S.P. Singh, K. Sreenivas, B.D. Malhotra, V. Gupta, Nanoporous cerium oxide thin film for glucose biosensor, *Biosens. Bioelectron.* 24 (2009) 2040–2045.
- [10] S.Y. Lu, D. Wu, Q.L. Wang, J. Yan, A.G. Buekens, K.F. Cen, Photocatalytic decomposition on nano-TiO₂: destruction of chloroaromatic compounds, *Chemosphere* 82 (2011) 1215–1224.
- [11] H. Park, W.R. Kim, H.T. Jeong, J.J. Lee, H.G. Kim, W.Y. Choi, Fabrication of dye-sensitized solar cells by transplanting highly ordered TiO₂ nanotube arrays, *Solar Energy Mater. Solar Cells* 95 (2011) 184–189.
- [12] Y. Jia, L. He, Z. Gio, X. Chen, F. Meng, T. Luo, M. Li, J. Liu, Preparation of porous tin oxide nanotubes using carbon nanotubes as templates and their gas-sensing properties, *J. Phys. Chem. C* 113 (2009) 9581–9587.
- [13] S.J. Bao, C.M. Li, J.F. Zang, X.Q. Cui, Y. Qiao, J. Guo, New nanostructured TiO₂ for direct electrochemistry and glucose sensor applications, *Adv. Funct. Mater.* 18 (2008) 591–599.
- [14] C.P. Sousa, A.S. Polo, R.M. Torresi, S.I. Torresi, W.A. Alves, Chemical modification of a nanocrystalline TiO₂ film for efficient electric connection of glucose oxidase, *J. Colloid Interface Sci.* 346 (2010) 442–447.
- [15] M. Viticoli, A. Curulli, A. Cusma, S. Kaciulis, S. Nunziante, L. Pandolfi, F. Valentini, G. Padeletti, Third-generation biosensors based on TiO₂ nanostructured films, *Mater. Sci. Eng. C* 26 (2006) 947–951.
- [16] J.P. Salvetat, J.M. Bonard, N.H. Thomson, A.J. Kulik, L. Forró, W. Benoit, L. Zuppiroli, Mechanical properties of carbon nanotubes, *Appl. Phys. A* 69 (1999) 255–260.
- [17] J. Zhao, A. Buldum, J. Han, J.P. Lu, First principles study of Li intercalated carbon nanotube ropes, *Phys. Rev. Lett.* 85 (2000) 1706–1709.
- [18] M. Kaempgen, C.K. Chan, J. Ma, Y. Cui, G. Gruner, Printable thin film supercapacitors using single-walled carbon nanotubes, *Nano Lett.* 9 (2009) 1872–1876.
- [19] N. Peng, Q. Zhang, C.L. Chow, O.K. Tan, N. Marzari, Sensing mechanisms for carbon nanotube based NH₃ gas detection, *Nano Lett.* 9 (2009) 1626–1630.
- [20] C.L. Cao, C.G. Hu, L. Fang, S.X. Wang, Y.S. Tian, C.Y. Pan, Humidity sensor based on multi-walled carbon nanotube thin films, *J. Nanomater.* 2011 (2011), 707303.
- [21] D. Odaci, A. Telefoncu, S. Timur, Pyranose oxidase biosensor based on carbon nanotube (CNT)-modified carbon paste electrodes, *Sens. Actuators B: Chem.* 132 (2008) 159–165.
- [22] W.J. Lee, E. Ramasamy, D.Y. Lee, J.S. Song, Efficient dye-sensitized solar cells with catalytic multiwall carbon nanotube counter electrodes, *ACS Appl. Mater. Interfaces* 1 (2009) 1145–1149.
- [23] Q. Shen, S.K. You, S.G. Park, H. Jiang, D. Guo, B. Chen, X. Wang, Electrochemical biosensing for cancer cells based on TiO₂/CNT nanocomposites modified electrodes, *Electroanalysis* 20 (2008) 2526–2530.
- [24] M. Tasvir, H.A.R. Pour, H. Ghourchian, M.R. Gholami, Amine functionalized TiO₂ coated on carbon nanotube as a nanomaterial for direct electrochemistry of glucose oxidase and glucose biosensing, *J. Mol. Catal. B: Enzym.* 68 (2011) 206–210.
- [25] S.V. Pammi, A. Chanda, J.K. Ahn, J.H. Park, C.R. Cho, W.J. Lee, S.G. Yoon, Low resistivity ITO thin films deposited by NCD technique at low temperature: variation of tin concentration, *J. Electrochem. Soc.* 157–10 (2010) H937–H941.
- [26] S. Lefrant, I. Baltog, M. Baibarac, Surface-enhanced Raman scattering studies on chemically transformed carbon nanotube thin films, *J. Raman Spectrosc.* 36 (2005) 676–698.
- [27] M.S. Dresselhaus, G. Dresselhaus, R. Saito, A. Jorio, Raman spectroscopy of nanotubes, *Phys. Rep.* 409 (2005) 47–99.
- [28] S. Shanmugam, A. Gabashvili, D.S. Jacob, J.C. Yu, A. Gedanken, Synthesis and characterization of TiO₂@C coreshell composite nanoparticles and evaluation of their photocatalytic activities, *Chem. Mater.* 18 (2006) 2275–2282.
- [29] P. Si, S. Ding, J. Yuan, X.W. Lou, D.H. Kim, Hierarchically structured one dimensional TiO₂ for protein immobilization, direct electrochemistry and mediator free glucose sensing, *ACS Nano* 5 (2011) 7617–7626.
- [30] Y. Lin, F. Lu, Y. Tu, Z. Ren, Glucose biosensors based on carbon nanotube nanoelectrode ensembles, *Nano Lett.* 4 (2004) 191–195.
- [31] S.A. Miscorora, G.D. Barrera, G.A. Rivas, Glucose biosensors based on the immobilization of glucose oxidase and polytyramine on rodhized glassy carbon and screen printed electrodes, *Sens. Actuators B: Chem.* 115 (2006) 205–211.
- [32] Z. Yang, Z. Ye, B. Zhao, X. Zong, P. Wang, A rapid response time and highly sensitive amperometric glucose biosensor based on ZnO nanorod via citric acid-assisted annealing route, *Physica E* 42 (2010) 1830–1833.
- [33] Z. Zhang, Y. Xie, Z. Liu, F. Rong, Y. Wang, D. Fu, Covalently immobilized biosensor based on gold nanoparticles modified TiO₂ nanotube arrays, *J. Electroanal. Chem.* 650 (2011) 241–247.
- [34] X. Pang, D. He, S. Luo, Q. Cai, An amperometric glucose biosensor fabricated with Pt nanoparticle-decorated carbon nanotubes/TiO₂ nanotube arrays composite, *Sens. Actuators B: Chem.* 137 (2009) 134–138.

- [35] Z. Wen, S. Ci, J. Li, Pt nanoparticles inserting in carbon nanotube arrays: nanocomposites for glucose biosensors, *J. Phys. Chem. C* 113 (2009) 13482–13487.
- [36] X. Liua, L. Shi, W. Niua, H. Li, G. Xu, Amperometric glucose biosensor based on single-walled carbon nanohorns, *Biosen. Bioelectron.* 23 (2008) 1887–1890.

Biographies

Nguyen Quoc Dung received his master of materials science in International Training Institute for Materials Science (ITIMS) at Hanoi University of Technology, Vietnam, in 2006. He is now in Ph.D. course in materials science and engineering, Chungnam National University, Korea. His current interests are nano-structure materials and their applications to bio- and chemical-sensors.

Dewyani Patil is a post doctoral fellow in Department of Materials Science and Engineering, Chungnam National University, Daejeon, South Korea. She did her Ph.D. in physics from North Maharashtra Univeristy, Jalgaon, India in 2010. Her research interests are synthesis of nanostructured materials and their application to gas sensors, biosensors and humidity sensors.

Thanh-Tung Duong is currently doing master course in Chungnam National University, Korea. His current research interests are photo-electrochemical cells and DSSC.

Hyuck Jung received his degree in master of materials science and engineering from Kumoh National University, Korea, in 2005. He is currently a Ph.D. scholar in materials science and engineering at Chungnam National University, Korea. His current interests include fabrication and characterization of carbon nanotube and its application to nano-electronic devices of transparent conductive film.

Dojin Kim received his Ph.D. in materials science and engineering from the University of Southern California, USA, in 1989. He is a professor at the School of Nanotechnology and the Department of Materials Science and Engineering in Chungnam National University, Korea. His current research interests are synthesis of carbon nanotube and metal oxides and applications to electronic devices of field emitters, solar cells, and gas sensors, so on. He is also interested in semiconductor nanostructures growth and applications.

Soon-Gil Yoon received his Ph.D. from the Korea Advanced Institute of Science and Technology, Korea in 1988. He is a professor in materials science and engineering, Chungnam National University, Korea. His current research interests are ferroelectrics, DRAM, transparent and dielectric materials, solar cell, nanowires as gas sensors, PRAM, graphene, etc.